# Synthesis, Structural, Magnetic, and Electrical Study of $BaSrCo_2O_5$, a Highly Disordered Cubic Perovskite

K. Boulahya,[†] J.C. Ruiz-Morales,[‡] M. Hernando,[†] J.M. González-Calbet,[†] and M. Parras*,[†]

*Departamento de Química Inorgánica, Facultad de Químicas, Universidad Complutense de Madrid, E-28040-Madrid, Spain, and Departamento de Química Inorgánica, Universidad de la Laguna, 38200, Canary Islands, Spain*

*Received September 25, 2008. Revised Manuscript Received March 13, 2009*

The influence of the partial substitution of Sr by Ba in the $SrCoO_{3-y}$ on its structure and properties has been investigated. $SrBaCo_2O_5$ is stable at room temperature as a cubic phase with a high oxygen vacancy concentration. This structure is stable up to 800 K. Above this temperature, the phase decomposes into a monodimensional rhombohedral $(SrBa)_7Co_6O_{18}$ phase. At 1200 K, a reversible rhombohedral → cubic transformation is observed, the rhombohedral phase remaining stable until room temperature. $SrBaCo_2O_5$ shows antiferromagnetic behavior with $T_N \approx 525$ K. As determined by neutron diffraction data, the magnetic Co spins align ferromagnetically on the (111) planes and these planes are stacked antiferromagnetically in the normal direction (type II antiferromagnet). The temperature dependence of the electrical conductivity indicates $SrBaCo_2O_5$ to be a semiconducting p-type material with an activation energy of ~0.3 eV.

## Introduction

Magnetic, electrical, and catalytic properties of cobaltites make them promising materials for different applications. The richness of the physical properties of cobaltites is related to the ability of Co ions to adopt not only several oxidation states but also various spin states. This is well-known in the case of the $LaCoO_3$ perovskite, where Co(III) exhibits spin-state transitions as a function of the temperature.[1,2] The alkaline-earth-doped cobaltite systems have also been extensively studied because of their interesting physical properties. For instance, besides the noticeable electrical properties of the $La_{1-x}Sr_xCoO_{3-y}$ system,[3] giant magnetoresistance has been reported in $La_{1-x}(Ba,Sr,Ca)_xCoO_{3-y}$.[4]

When either Sr or Ba fully occupy the perovskite A sublattice, two structurally different perovskites are obtained. $SrCoO_3$, prepared under high oxygen pressure, corresponds to a cubic perovskite.[5,6] This three-dimensional structure is formed by $[CoO_6]$ octahedra sharing corners. Since cobalt can adopt different oxidation states in various oxygen environments, several anionic deficient phases can be established. $SrCoO_{3-y}$[7,8] belongs to the family of non stoichiometric perovskites showing high oxygen mobility even at room temperature, making $SrCoO_{3-y}$ a promising candidate for use in catalysis, gas sensing material or cathodes for oxide fuel cells (SOFCs).[9,10] The cubic structure of $SrCoO_{3-y}$ changes to the orthorhombic brownmillerite-type structure for $SrCoO_{2.50}$.[11] The oxygen stoichiometry can be modified by controlling the temperature and/or the oxygen partial pressure, but also by electrochemical oxidation. In this sense, the structural changes occurring during the electrochemical oxidation of $SrCoO_{2.50}$ to $SrCoO_3$ have been recently investigated and two new ordered phases have been found for $SrCoO_{2.82}$ and $SrCoO_{2.75}$.[12] These compositional and structural changes drastically affect the magnetic and transport properties of these materials. $SrCoO_3$ exhibits ferromagnetism $T_C$ close to 266 K[13] and metallic electric conductivity, whereas $SrCoO_{2.50}$ is an antiferromagnetic and charge-transfer insulator material.[14]

The partial substitution of Sr by Ca does not significantly modify the structural and physical properties of $SrCoO_3$. In this sense, although stoichiometric $CaCoO_3$ has not been

* Corresponding author. E-mail: mparras@quim.ucm.es. Fax: (34) 91 394 43 52.
[†] Universidad Complutense de Madrid.
[‡] Universidad de la Laguna.

(1) Harrison, W.; Hedwood, S. L.; Jacobson, A. J. *J. Chem. Soc., Chem. Commun.* **1995**, 1953.
(2) Podlesnyak, A.; Streule, S.; Mesot, J.; Medarde, M.; Pomjakushina, E.; Conder, K.; Tanaka, A.; Haverkort, M. W.; Khomskii, D. I. *Phys. Rev. Lett.* **2006**, *97*, 247208.
(3) Petrov, A. N.; Kononchuk, O. F.; Andreev, A. V.; Cherepanov, V. A.; Kofstad, P. *Solid State Ionics* **1995**, *80*, 189.
(4) Briceno, G.; Xiang, X. D.; Change, H.; Sun, X.; Schultz, P. G. *Science* **1995**, *270*, 273.
(5) Wang, X. L.; Sakurai, H.; Takayama-Muromachi, E. *J. Appl. Phys.* **2005**, *97*, 10M519.
(6) Deng, Z. Q.; Yang, W. S.; Liu, W.; Chen, C. S. *J. Solid State Chem.* **2006**, *179*, 362.
(7) Grenier, J. G.; Ghodbane, S.; Demazeau, G.; Pouchard, M.; Hagenmuller, P. *Mater. Res. Bull.* **1979**, *14*, 831.
(8) Takeda, Y.; Kanno, R.; Takada, T.; Yamamoto, O.; Takano, M.; Bando, Y. *Z. Anorg. Allg. Chem.* **1986**, *259*, 540.
(9) Boehm, E.; Bassant, J. M.; Steil, M. C.; Dordor, P.; Mauvy, F.; Grenier, J. C. *Solid State Ionics* **2003**, *5*, 973.
(10) Lang, Y.; Chen, C. L.; Chen, S. Y.; Chu, C. W.; Jacobson, A. J. *Electrochem. Soc.* **2000**, *174* (11), 4001.
(11) Takeda, T.; Yamaguchi, Y.; Watanabe, H.; Tomiyoshi, S.; Yamamoto, H. *J. Phys. Soc. Jpn.* **1969**, *26*, 1320.
(12) Le Toquin, R.; Paukus, W.; Cousson, A.; Prestipino, C.; Lamberti, C. *J. Am. Chem. Soc.* **2006**, *128*, 13161.
(13) Mathi Jaya, S.; Jagadish, R.; Rao, R. S.; Asokamani, R. *Phys. Rev. B* **1991**, *43* (16), 13274.
(14) Pardo, V.; Botta, P. M.; Baldomir, D.; Rivas, J.; Piñeiro, A.; de la Calle, C.; Alonso, J. A.; Arias, J. E. *Phys. B: Condens. Matt.* **2008**, *403*, 1636.

10.1021/cm802606s CCC: $40.75 
Published on Web 04/30/2009

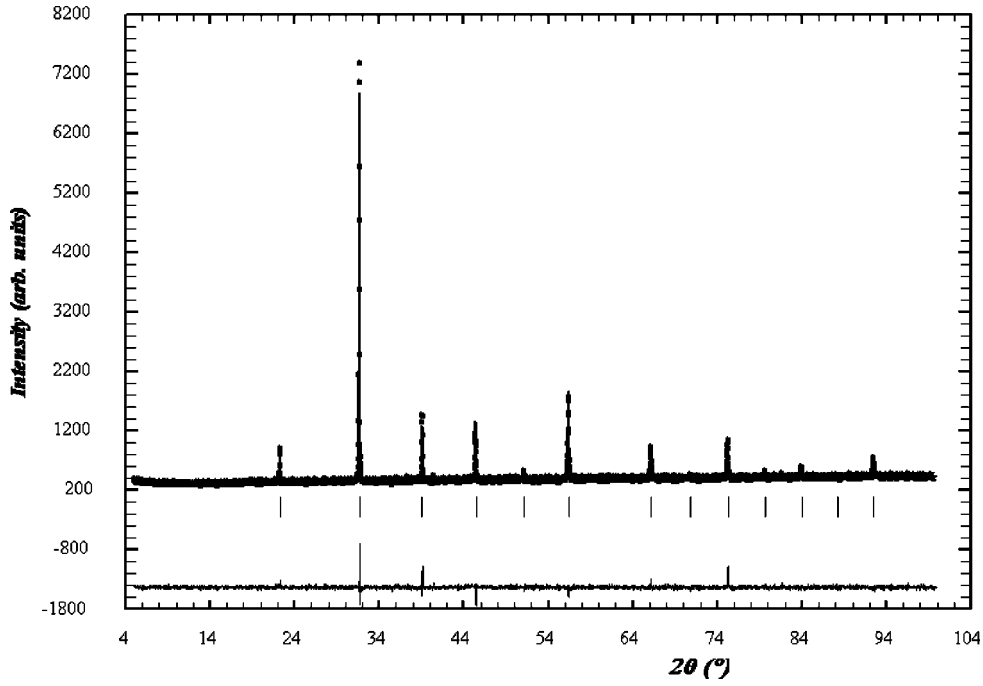


**Figure 1.** Graphic results of the fitting of the powder XRD data of $SrBaCo_2O_5$: experimental (points), calculated (solid line), and difference (bottom).

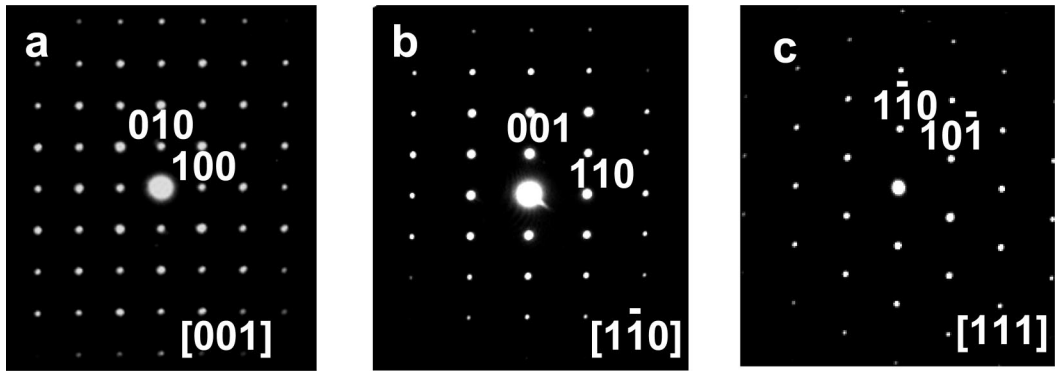


**Figure 2.** SAED patterns corresponding to $SrBaCo_2O_5$: (a) [001], (b) [1$\bar{1}$0], and (c) [111] zone axes.

isolated previously, different samples in the $Sr_{1-x}Ca_xCoO_3$[15] ($0 \leq x \leq 0.8$) system have been recently stabilized under high temperature and pressure conditions. All of them maintain the cubic perovskite structure and exhibit ferromagnetism. However, when Sr is replaced by Ba, important structural modifications take place. $BaCoO_3$[16] is a structurally one-dimensional compound because it crystallizes in the hexagonal perovskite 2H-structure, formed by chains of face-sharing [$CoO_6$] octahedra. Unlike the higher symmetry isoelectronic $SrCoO_3$, $BaCoO_3$ is not metallic but semiconductor. To the best of our knowledge, $BaCoO_{2.50}$ has not been yet stabilized; however, a preliminary work on $Sr_{1-x}Ba_xCoO_{2.5}$[17] has been reported and, although neither microstructural characterization nor physical properties have been investigated, it seems that single cubic materials are formed in the $0.2 \leq x \leq 0.5$ range. This feature seems to indicate a random distribution of the vacancies through the anionic sublattice of the perovskite structure. This is an amazing result because such a high vacancy concentration usually gives rise to the stabilization of ordered phases. In this sense, for an $ABO_{2.5}$ stoichiometry, different prototypes of oxygen vacancy ordering have been reported characterized by partial or total replacement of the $MO_6$ octahedra in the perovskite by square planar $MO_4$, as in $LaNiO_{2.5}$,[18,19] tetrahedral $MO_4$ as in the brownmillerite $Ca(AlFe)O_{2.5}$[20] structure, or square pyramids $MO_5$ in $CaMnO_{2.5}$.[21]

The partial substitution of Sr by Ba should strongly influence the structural and physical properties of the $SrCoO_{2.5}$ brownmillerite type oxide. In this sense, it is worth recalling that from the point of view of their properties, in the $SrCoO_{3-y}$ system, high-temperature $SrCoO_{2.5}$ shows the highest electronic and oxygen ionic conductivity, with a maximum reported total electrical conductivity of 160 S $cm^{-1}$

(15) Balamurugan, S.; Xu, M.; Takayama-Muromachi, E. *J. Solid State Chem.* **2005**, *178* (11), 3431–3436.
(16) Felser, C.; Yamaura, K.; Cava, R. J. *J. Solid State Chem.* **1999**, *146*, 411–417.
(17) Yamamura, K.; Zandbergen, H. W.; Abe, K.; Cava, R. J. *J. Solid State Chem.* **1999**, *146*, 96–102.
(18) Gai, P. L.; Rao, C. N. R. *Z. Naturforsch., A* **1975**, *30*, 1092.
(19) González-Calbet, J. M.; Sayagués, M. J.; Vallet-Regí, M. *Solid State Ionics* **1989**, *32* (32), 72.
(20) Bertaut, E. F.; Blum, P.; Sagnieres, A. *Acta Crystallogr.* **1959**, *12*, 149.
(21) Poeppelmeier, K. R.; Leonowicz, M. E.; Longo, J. M. *J. Solid State Chem.* **1982**, *44* (1), 89–98.

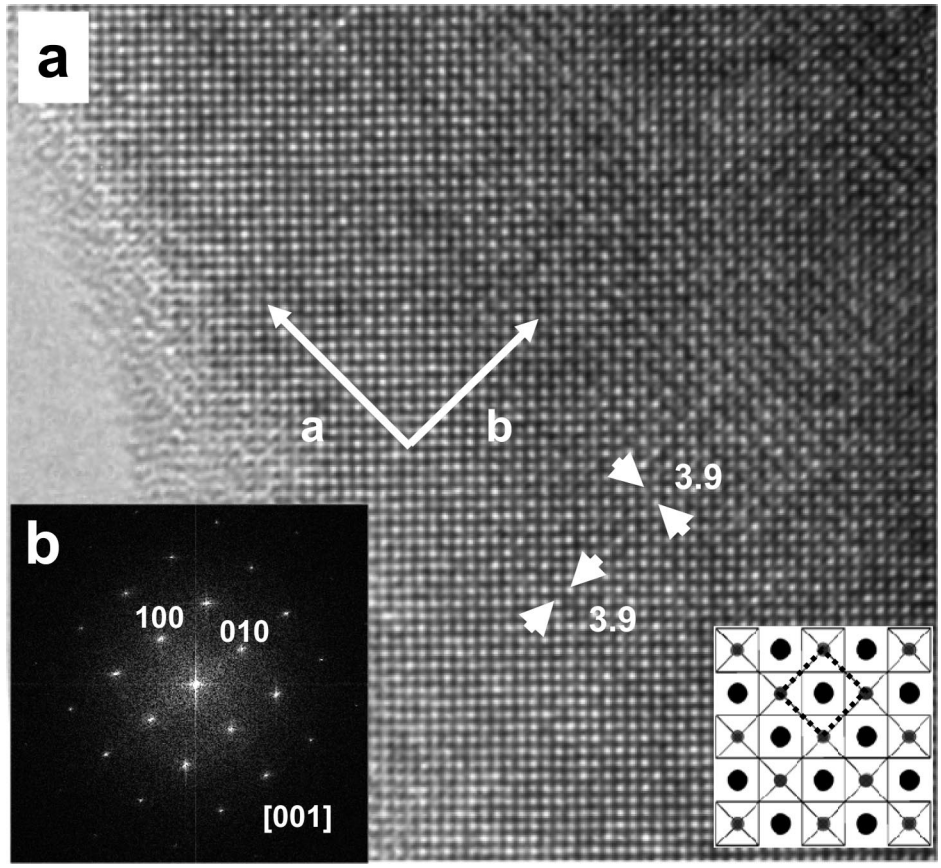


**Figure 3.** (a) HREM image of $SrBaCo_2O_5$ along [001], (b) corresponding FT. Structural model is depicted in the inset.

at temperature close to 1223 K.[22] At this temperature, the anionic vacancies in $SrCoO_{2.5}$ are not ordered and the phase symmetry changes from orthorhombic to cubic. From this, much effort has been made to stabilize this cubic phase at room temperature. In particular, the strategy of the cationic substitution has been extensively applied, mainly in the B sublattice because the B-site doping seems to be more favorable for preserving high oxygen-vacancy concentrations. The aim of this work is to determine the influence of the $Ba^{2+}$ doping in the A site of $SrCoO_{2.5}$ on its structure and physical properties. This work shows that the anionic stoichiometry as well as the cubic symmetry of the high-temperature $SrCoO_{2.5}$ phase can be stabilized at room temperature by the partial substitution of Sr by Ba on the A cationic sublattice. In this paper, we report the structural characterization, phase stability, and physical properties of $SrBaCo_2O_5$.

## Experimental Section

Polycrystalline $SrBaCo_2O_5$ was synthesized in a Pt crucible by heating stoichiometric amounts of $SrCO_3$ (Aldrich 99.98%), $Co_3O_4$ (Aldrich 99.9%), and $BaCO_3$ (Aldrich 99+%) in air at 1473 K for 7 days, and then quenching it to room temperature in air.

The average cationic composition was determined by inductive coupling plasma (ICP), whereas the local composition was analyzed by energy-dispersive X-ray spectroscopy (EDS) with an INCA analyzer system attached to a JEOL 3000 FEG electron microscope. The oxygen content was determined by thermogravimetric analysis on a Cahn D-200 electrobalance where the oxygen content can be determined within $\pm 5 \times 10^{-3}$ for a sample of total mass of about 50 mg.

The powder X-ray diffraction (XRD) pattern at room temperature (RT) was collected using Cu K$\alpha$ radiation ($\lambda = 1.5418$ Å) on a PHILIPS X'PERT diffractometer equipped with a graphite monochromator. High-temperature powder XRD data at air were carried out on Panalytical X'PERT PRO diffractometer supplied with a X'Celerator fast detector and Ni $k_\beta$-filter with Cu K$\alpha$ radiation. Neutron powder diffraction (NPD) data were collected at room temperature and 573 K on the high-resolution powder diffractometer D2B at the Institute Laue Langevin (ILL), Grenoble, France, with neutrons of wavelength 1.594 Å. The angular range covered by the detector expands from 0 to 160° in scattering angle (step size 0.05°). At 573 K, data were collected with the sample loaded in a quartz tube open at ambient atmosphere placed in a furnace. Diffraction data were analyzed by the Rietveld[23] method using the Fullprof program.[24]

The sample was characterized by selected area electron diffraction (SAED) and high-resolution electron microscopy (HREM) by using a Jeol 3000 FEG electron microscope, fitted with a double tilting goniometer stage (±20°, ±20°). Local composition was analyzed by energy-dispersive X-ray spectroscopy (EDS) with an Oxford analyzer system attached to the above-mentioned electron microscope.

DC magnetization was measured in a Quantum Design PPMS in a temperature range from 1.8 to 650 K under an applied magnetic field up to 1 KOe.

Pellets for impedance measurements, 0.79 mm thick and 6.03 mm diameter, were obtained by uniaxially pressing $SrBaCo_2O_5$ powders

(22) Nagai, T.; Ito, W.; Sakon, T. *Solid State Ionics* **2007**, *177*, 3433.

(23) Rietveld, H. M. *J. Appl. Crystallogr.* **1969**, *2*, 65.
(24) Rodríguez-Carvajal, J. *Physica B* **1993**, *192*, 55.

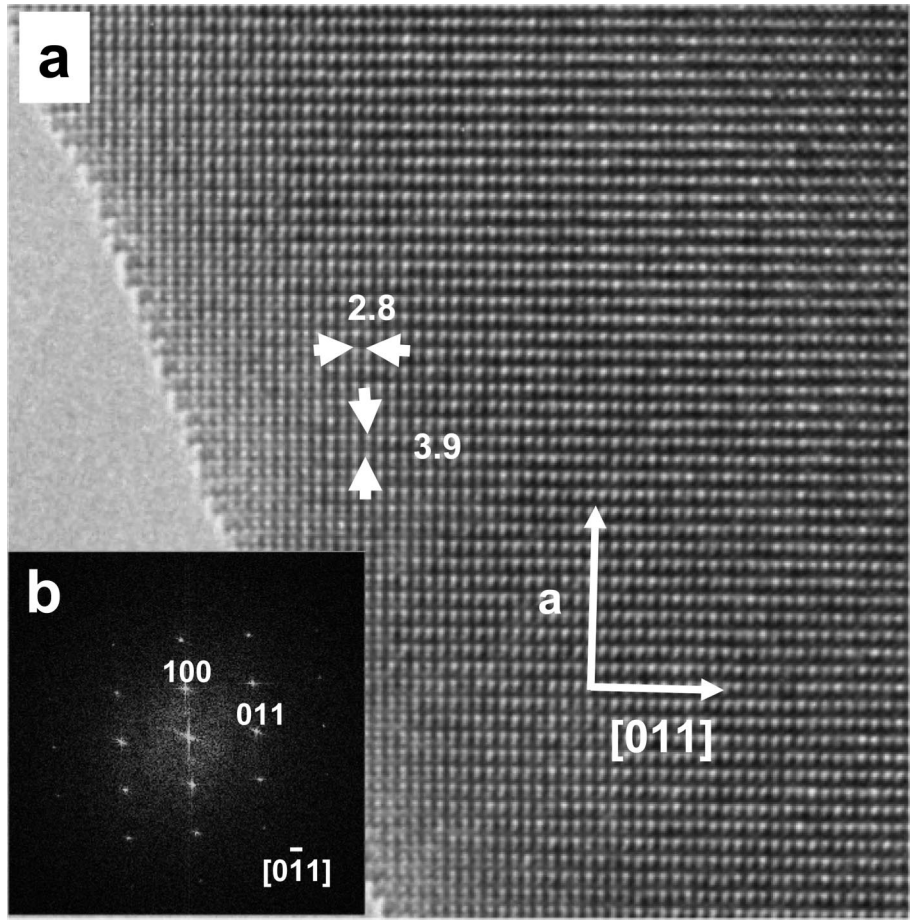


**Figure 4.** (a) HREM image of $SrBaCo_2O_5$ along [1$\bar{1}$0]; (b) corresponding FT.

at 30 MPa for 2 min. The resulting pellets were not further sintered because of the instability at temperatures above 523 K; consequently, the relative density was low, i.e., 64% of the theoretical density. The conductivity values were corrected with the relative density of the sample. The pellet was fixed in an electrochemical setup of alumina with Pt wires for the electrical connections and then inserted into a quartz flow-through tube furnace.

The conductivity measurements were performed by electrochemical impedance spectroscopy with a Solartron 1260 frequency response analyzer (FRA), at open circuit voltage (OCV), in the frequency range $1 \times 10^6$ to $1 \times 10^{-1}$ Hz, using a 50 mV amplitude a.c. signal, obtaining reproducible spectra. The measurements were performed on a two-electrode arrangement under symmetric atmospheres, using oxygen, Ar, and finally 5% $H_2-Ar$ to test the sample stability under reducing conditions. The sample was first heated to 523 K until the thermal equilibrium was reached. Impedance spectra were recorded every ~25 K, on cooling.

## Results and Discussion

The cationic composition, determined on several dozens of small crystallites by energy dispersive X-ray analysis in the electron microscope, is in agreement with the nominal one. The oxygen content was determined by thermogravimetric analysis by reduction under 200 mbar $H_2$/300 mbar He atmosphere and heating at 6 K/min up to 1123 K. BaO, SrO and Co metal were identified by XRD as the final products of the reduction process. The observed weight-loss, corresponding to 11.5% of the starting material, leads to the $BaSrCo_2O_{5.00(5)}$ composition.

**Phase Structure.** The sample of nominal composition $SrBaCo_2O_5$ was confirmed to be single phase by XRD. The whole pattern can be indexed on the basis of a cubic unit cell with lattice parameter $a = 3.933(4)$ Å (Figure 1), no extra reflections being detected. This is a quite surprising result because the lack of one oxygen atom every six in a perovskite related structure usually leads to ordering on the anionic sublattice, as observed in the brownmillerite type of $SrCoO_{2.5}$.[11] To look for a kind of additional ordering, we have performed an electron microscopy study.

Selected area electron diffraction (SAED) has been used to fully reconstruct the reciprocal space. In Figure 2, the most relevant zone axes, [001], [1$\bar{1}$0], and [111] are depicted. All reflections correspond to a basic cubic perovskite cell. No additional spots are observed. Actually, all the maxima can be indexed on the basis of a simple cubic perovskite unit cell with parameter $a = a_p \approx 3.9$ Å. Besides, the reflection conditions are compatible with the $Pm\bar{3}m$ (225) space group, previously proposed for other cubic perovskites.

The most relevant images are shown in Figures 3a, 4a, and 5a. The HREM micrograph along [001] (Figure 3a) shows an apparently well-ordered material with *d*-spacings of 3.9 Å, corresponding to $d_{100}$ and $d_{010}$. Fourier transform was performed on the HREM micrograph, looking for the existence of different domains that could show the presence of additional ordering of the structure (cationic or anionic). However, the whole crystal results are homogeneous and only the maxima corresponding to the simple cubic perovs-

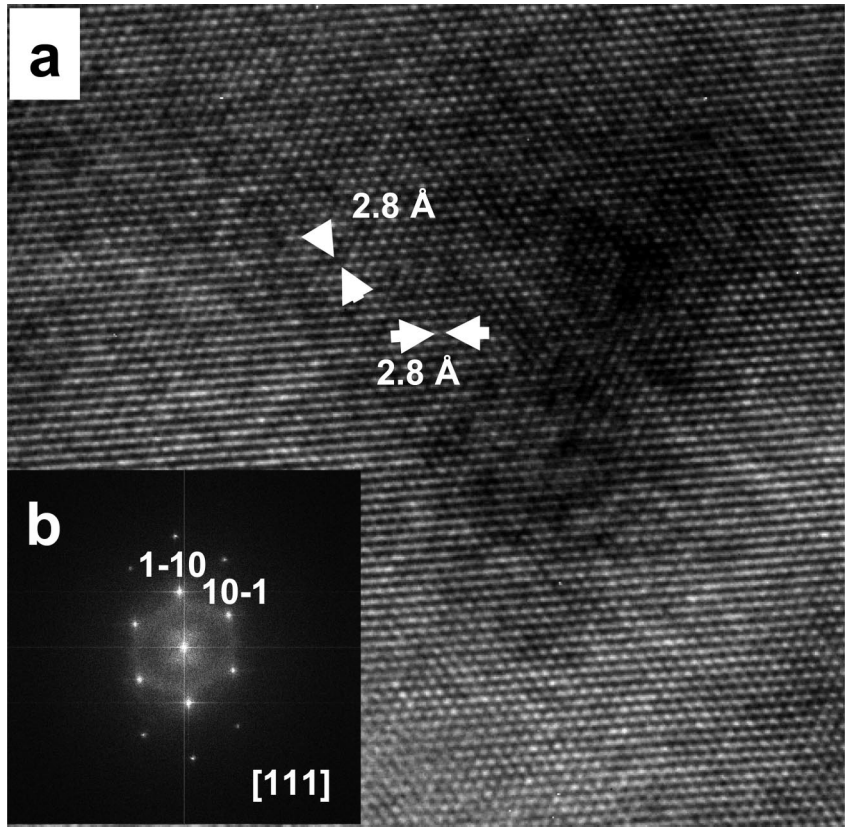


**Figure 5.** (a) HREM image of $SrBaCo_2O_5$ along [111]; (b) corresponding FT.

kite were observed (Figure 3b). The contrast observed in this image corresponds to bright dots alternating with the brightest one, which can be associated with the Ba/Sr atoms alternating with Co ones along $[1\bar{1}0]$ as shown in the structural model depicted in the inset of Figure 3a. The lack of additional ordering in the cubic structure is also evidenced in the HREM of Figures 4a and 5a taken along the $[1\bar{1}0]$ and [111] zone axes. Besides, the corresponding Fourier transforms (Figures 4b and 5b) show only the diffraction maxima of a simple cubic phase.

According to that, the structural model for $SrBaCo_2O_5$ results in an oxygen deficient perovskite structure with random distribution of anionic vacancies. This model was considered as the starting one in the $Pm\bar{3}m$ for the XRD refinement at room temperature. The resulting structural parameters are listed in Table 1. The graphical result of the refinement is shown in Figure 1. A good fit between calculated and experimental data was achieved, as highlighted by the low *R*-values.

These results show that the presence of large-size $Ba^{2+}$ in the A sublattice leads to the efficient stabilization of the cubic HT-$SrCoO_{2.5}$ phase at room temperature. SAED and HREM show the lack of extra order, suggesting a random distribution of both Ba/Sr in the cationic sublattice and oxygen vacancies in the anionic one.

**Thermal Stability.** It is well-known that $SrCoO_{2.5}$, brownmillerite type, is metastable at room temperature and can indeed be obtained only by quenching from high temperature into liquid nitrogen. Slow cooling gives rise to the decomposition of the brownmillerite phase into $Sr_6Co_5O_{15}$[25] and $Co_3O_4$. Besides, above 1073 K, a cubic perovskite-type phase is stabilized. The structural evolution of $SrCoO_{2.5}$ brownmillerite-like phase from room temperature to 1475 K has been recently revisited.[26] As opposite to the studied phase $SrBaCo_2O_5$, in this system, only at high temperature are the anionic vacancies not long-range ordered.

**Table 1. Structural Parameters for $SrBaCo_2O_5$ obtained from the Refinement of Neutron Diffraction and X-ray Data**

| | 300 K | | 573 K |
|---|---|---|---|
| | XR | ND | ND |
| *a* (Å) | 3.98962(14) | 3.983284(13) | 4.00186(9) |
| | Sr/Ba (1/2, 1/2, 1/2) | | |
| $B_{iso}$ (Å$^2$) | 0.49(14) | 1.675 (17) | 2.21(8) |
| $f_{occ}$ | 0.5/0.5 | 0.5/0.5 | 0.5/0.5 |
| | Co (0,0,0) | | |
| $B_{iso}$ (Å$^2$) | 0.698(22) | 1.736(17) | 2.57(8) |
| $f_{occ}$ | 1 | 1 | 1 |
| $M$ ($\mu_B$) | | 2.5(2) | |
| | O (1/2,0,0) | | |
| $B_{iso}$ (Å$^2$) | 5.7(7) | 3.676(17) | 4.291(9) |
| $f_{occ}$ | 0.83 | 0.833(3) | 0.833(4) |
| $\chi^2$ | 1.87 | 5.20 | 2.04 |
| $R_p$(%) | 4.47 | 2.16 | 5.20 |
| $R_{wp}$(%) | 6.43 | 3.29 | 6.55 |
| $R_{exp}$(%) | 4.70 | 1.51 | 5.91 |
| $R_{Bragg}$(%) | 6.23 | 3.29 | 6.30 |
| $R_{mag}$(%) | | 4.40 | |

To investigate the thermal stability of cubic $Sr_{0.5}Ba_{0.5}CoO_{2.5}$, we have performed a detailed study by means of TGA and DTA and high-temperature X-ray and neutron diffraction. Figure 6 shows the TGA and DTA curves for $SrBaCo_2O_5$ carried out in

(25) Harrison, W.; Hedwood, S. L.; Jacobson, A. J. *J. Chem. Soc., Chem. Commun.* **1995**, 1953.
(26) de la Calle, C.; Aguadero, A.; Alonso, J. A.; Fernández-Díaz, M. T. *Solid State Sci.* **2008**, *10*, 1924.

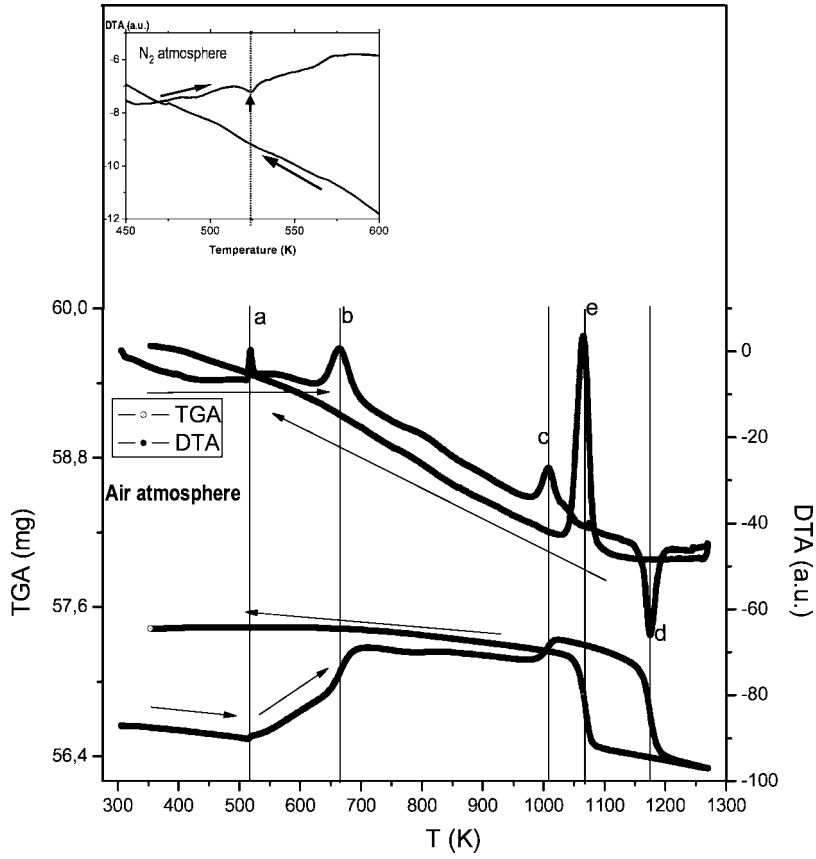


**Figure 6.** Thermal analysis curves collected in air for $SrBaCo_2O_5$: TGA (left axis); DTA (right axis). Inset: DTA measurements from 450 to 600 K under a $N_2$ atmosphere.

air. In the experimental temperature range (RT to 1173 K), three exothermic and one endothermic peaks are observed in the heating process, whereas only one exothermic peak is visible in the cooling process.

The first peak at $T \approx 515$ K (a) is related to a magnetic transition from an antiferromagnetic to a paramagnetic state (see below). By further heating, a broader peak (b) centered at about 660 K appears. The TGA curve shows a weight gain starting at about 520 K and increasing up 700 K that probably corresponds to an increase of the oxygen content (from 2.5 at RT to 2.66 at 700 K per unit formula). This oxidation process seems to occur without significant structural changes. Actually, Figure 7 shows the XRD patterns collected at different temperatures from RT to 1300 K. In the temperature region where the exothermic effect is observed (b), the essential features of the cubic phase are maintained and there is not evidence of some structural change that could be associated with such a peak. In fact, the cubic phase is stable until a temperature close to 800 K. Above this, extra reflections (marked with asterisks) appear corresponding to a rhombohedral phase belonging to the one-dimensional $((Sr-Ba)_3Co_2O_6)_\alpha$ $((Sr-Ba)_3Co_3O_9)_\beta$ family;[27] this phase is the visible only up to 1075 K. $Sr_2Co_2O_5$, undergoes a similar transformation with a phase segregation from brownmillerite to 1D rhombohedral $Sr_6Co_5O_{15}$ phase and $Co_3O_4$.[25] ($\alpha = 3$, $\beta = 3$ term of the series). In our case, the presence of Ba stabilizes a higher term of the series and the whole pattern at 1075 K corresponds to the $\alpha = 3$, $\beta = 4$ term of the series with a chemical composition close to $(SrBa)_7Co_6O_{18}$ as evidenced by the SAED pattern of Figure 8.[27] Therefore, the sharp exothermic peak at 1033 K (c) can be correlated to a decomposition process from the cubic to the 1D phase. The slight Co excess is not apparent in the XRD pattern.

By further heating of the sample, a very sharp endothermic peak is observed at 1173 K (d), which in the cooling run appears as an exothermic peak at $T$ close to 1073 K (e). The origin of this peak is the transformation of the rhombohedral 1D phase into a cubic phase as shown by the XRD patterns taken up to 1175 K. The TGA curve shows a weight loss according to the reduction process accompanying to the transformation from the 1D $(SrBa)_7Co_6O_{18}$ to a cubic $SrBaCo_2O_5$ related phase. This process is reversible, and by cooling below 1025 K, the rhombohedral phase is obtained and remains stable until room temperature. A similar change is observed for 1D $Sr_6Co_5O_{15}$ that transforms to a cubic 3C $SrCoO_{2.5}$ structure that, by cooling, is transformed again into the rhombohedral one.

**Physical Properties.** *Magnetic Properties.* Figure 9 shows the evolution of the field -cooled (FC) magnetic susceptibility versus temperature the the range 1.8−650 K under an applied field of 1000 Oe. The magnetic curve increases at temperatures higher than 150 K, tending toward a maximum located to ~525 K. However, no sharp transition was observed making difficult to accurately establish the magnetic transition temperature from these data. A similar behavior has been

(27) Boulahya, K.; Parras, M.; Gonzaléz-Calbet, J. M. *Chem. Mater.* **2000**, *12*, 25.

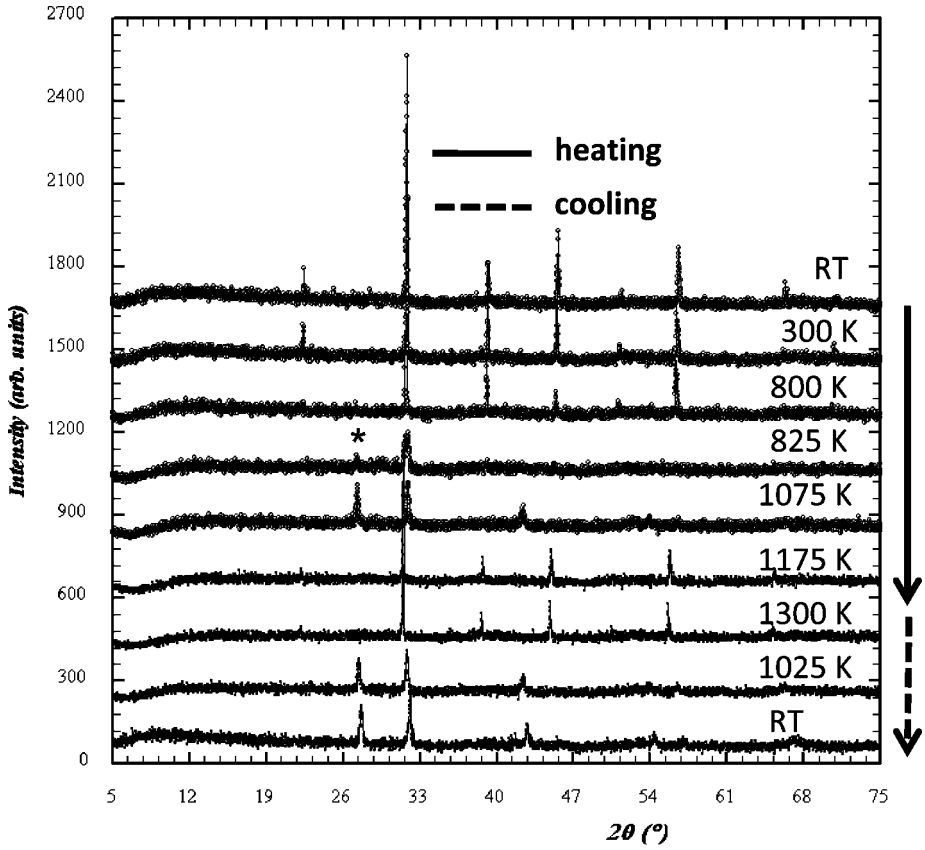


**Figure 7.** Thermal evolution of the XRD patterns collected in situ starting from $SrBaCo_2O_5$ cubic polymorph.

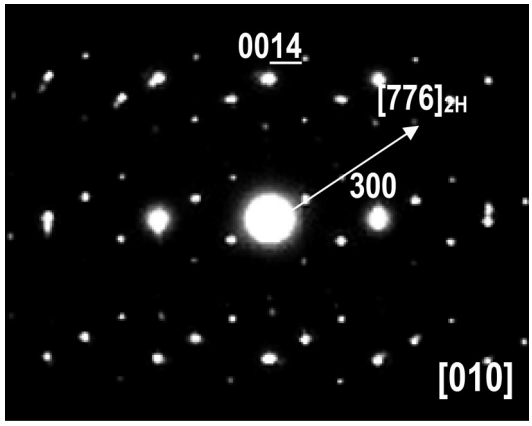


**Figure 8.** SAED pattern corresponding to $(SrBa)_7Co_6O_{18}$ along the [010] zone axis.

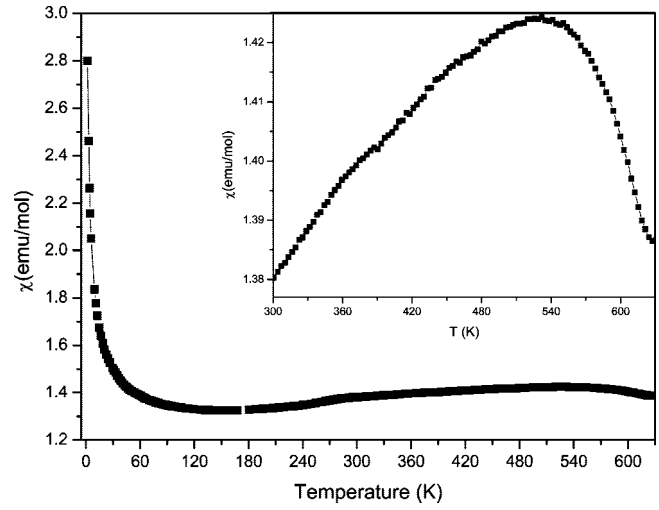


**Figure 9.** Magnetic susceptibility versus temperature for polycrystalline $SrBaCo_2O_5$.

found in $SrCoO_{2.5}$,[28] in which a broad maximum centered at ~570 K appears. This latter compound with brownmillerite structure presents an antiferromagnetic order below Neel temperature (~570 K). This order−disorder magnetic transition appears in the DTA curve as a weak endothermic peak.[26] In the Ba-doped sample around 520 K, a slight oxidation process begins leading to an exothermic peak in the corresponding DTA curve (see Figure 6), which could overlap the possible endothermic effect associated to a magnetic transition. Therefore, to avoid this, we carried out DTA measurements in a $N_2$ atmosphere from RT up to 600 K (inset at Figure 6). As can be observed, only an endothermic peak appears at temperature close to 520 K that should correspond to the magnetic transition. Therefore, although the structures of $SrBaCo_2O_5$ and $Sr_2Co_2O_5$ are clearly different, the features of the magnetic susceptibility could be due to the onset of the antiferromagnetic order between magnetic Co cations. Moreover, the higher $T_N$ in $SrBaCo_2O_5$, shows that a strong magnetic coupling is retained despite the significant structural disorder existing in the cubic phase.

Note that the transition from the paramagnetic (P) to the antiferromagnetic (AF) sate is not reflected in a sharp reduction but in a gradual decrease on the magnetic susceptibility in the temperature range from 575 to 400 K is observed. Although this feature is rather unusual, it could be related to the fully disordered anionic sublattice of $BaSrCo_2O_5$, which may involve different magnetic super-

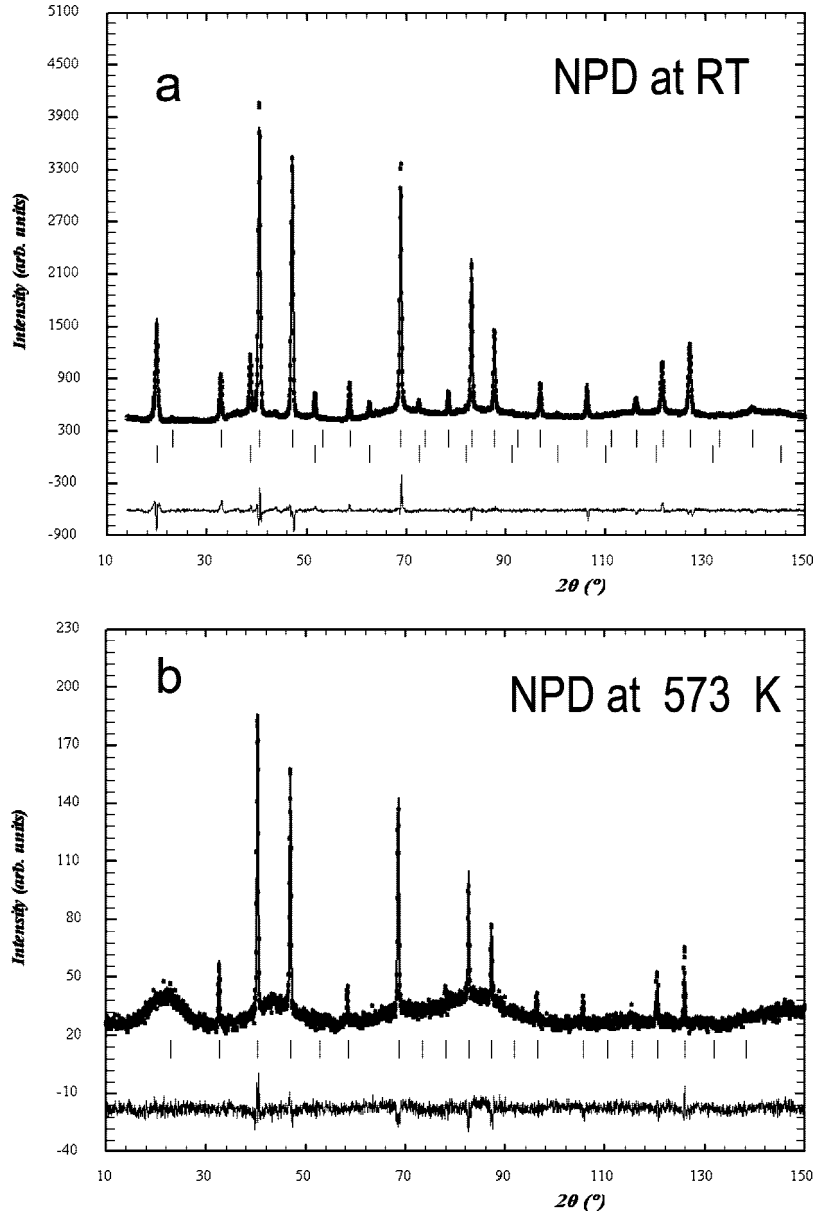


**Figure 10.** Graphic result of the fitting of the neutron powder diffraction data of $SrBaCo_2O_5$: at (a) RT and (b) 573 K: Experimental (points), calculated (solid line), and difference (bottom). The first series of tick marks in (a) correspond to the nuclear structure, whereas the second series corresponds to the magnetic satellites defined by the propagation vector $k = (1/2\ 1/2\ 1/2)$.

exchange pathways, giving rise to a large and slow order (AF)−disorder (P) transition.

To get more information about the magnetic features of this material we have carried out a NPD study. The high-resolution neutron diffraction data collected at 300 (RT) and 573 K, panels a and b in Figure 10, respectively, could be properly refined in spite of the irregular background coming from the quartz container. The refinement of the neutron diffraction pattern at 573 K (Figure 10b) confirms the XRD results, with all the maxima being indexed on a cubic cell of parameter $a = 4.00186(9)$Å, (SG: $Pm\bar{3}m$). Besides, the refined occupation factor for oxide positions gives a $Ba_{0.5}Sr_{0.5}CoO_{2.49(1)}$ anionic composition, in perfect agreement with the TGA results. The structural parameters obtained are gathered in Table 1.

On the contrary, the neutron diffraction pattern recorded at RT contains additional peaks corresponding to magnetic

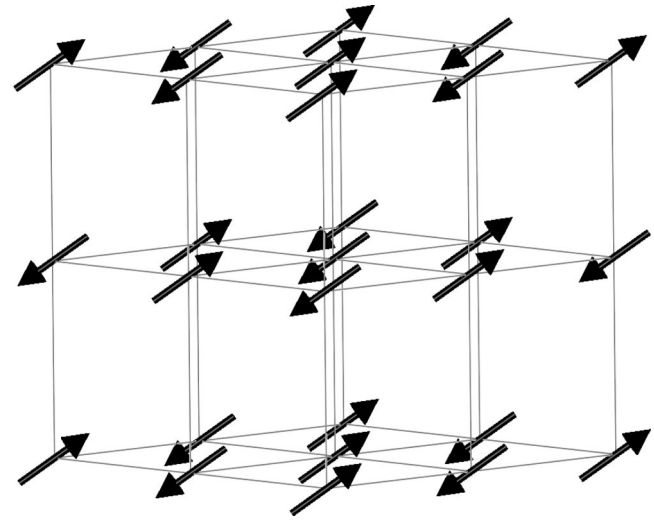

**Figure 11.** Magnetic structure of $SrBaCo_2O_5$. Only Co cations are shown.

(28) Takeda, T.; Watanabe, H. *J. Phys. Soc. Jpn.* **1972**, *33*, 973.

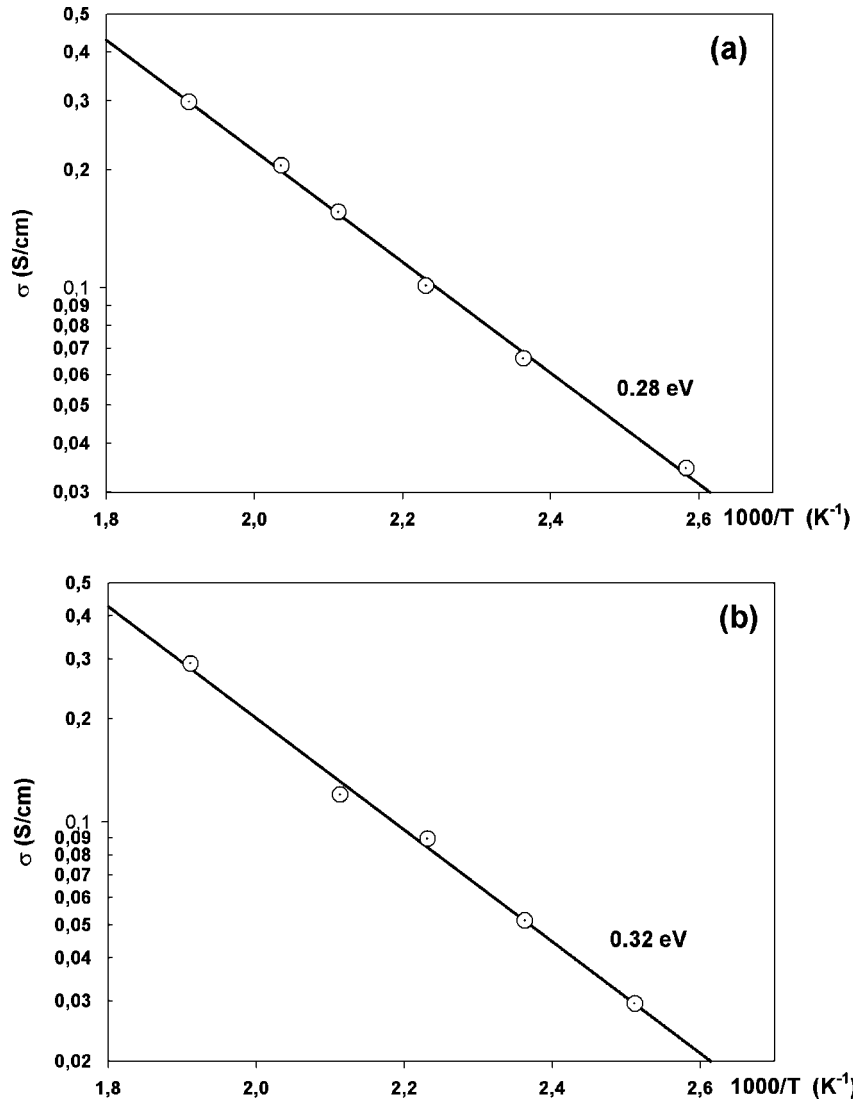


**Figure 12.** Arrhenius plot of $SrBaCo_2O_5$ under (a) $O_2$ and (b) Ar.

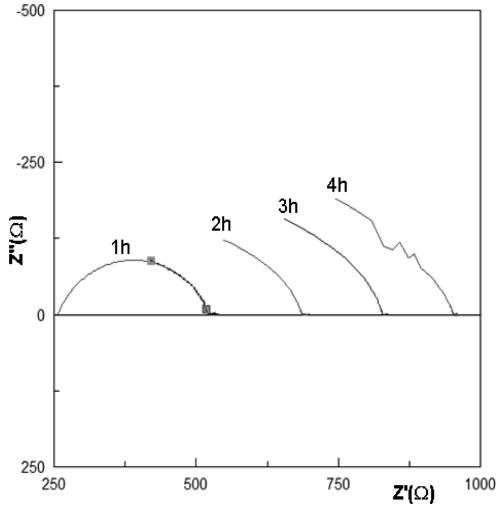


**Figure 13.** Impedance spectra obtained under $5H_2-Ar$ for several hours showing the instability of the material under reducing conditions at low temperature.

satellites defined by the propagation vector $k = (1/2\ 1/2\ 1/2)$. The starting magnetic model was obtained using the BasIreps program, included on the Fullprof Suite package.[24] The program provides a unique solution that has been used in the neutron diffraction refinement at RT. The only magnetic mode for $k = (1/2, 1/2, 1/2)$ and for the 1a site occupied by Co is the $\Gamma$ irreducible (1, 1, 1) representation. For this representation, the basis vectors for Co atoms can present magnetic component along *x*, *y*, and *z* directions; however, the refinement of the ND data shows that one of the component turns to be negligible, and therefore, the magnetic moments of the Co atoms are into one of the three *xz*, *yz*, or *yz* equivalents planes. The obtained magnetic component values are 1.94 and 1.57 $\mu_B$ and the magnetic moment modulus is 2.5(2) $\mu_B$/Co. The calculated and experimental patterns are shown in Figure 10a. The results of the refinement of the best fit are summarized in Table 1. As an example, in the magnetic structure depicted in Figure 11, the moments are lying in the *xz* plane pointing at 55° with respect to the *z*-axis.

The antiferromagnetic structure can be regarded as magnetic Co spins aligned ferromagnetically within {111} planes and these planes are antiferromagnetically coupled in the normal direction to a given (111) plane. The saturated magnetic moments of Co atoms are listed in Table 1, giving a total value of 2.5 (2)$\mu_B$. This value is somewhat lower than

the one obtained for $Sr_2Co_2O_5$, 3.3(5), probably because the saturation magnetic moment has not been reached yet at 300 K. The same magnetic order is established in cubic $Ba_2MnMoO_6$.[29] Actually, the magnetic structure of this cubic perovskite also consists of ferromagnetic (111) layers of magnetic cations coupled antiferromagnetically. In fact, this order corresponds to the well-known cubic MnO,[30] which presents the same cationic arrangement as that of Co in $SrBaCo_2O_5$ or Mn in $Ba_2MnMoO_6$.

*Electrical Conductivity.* The Nyquist plot under oxygen flow shows the inductance from the connecting wires and the overall resistance of the material highlighting the predominant electronic contribution of the sample and, therefore, it is not possible to discriminate bulk and grain boundary contributions. The overall resistance, under both oxygen and Ar atmospheres, was obtained from the fitting of the impedance data to an ideal equivalent circuit with two elements connected in series, L(Rs), where L is an inductance element and Rs is the overall resistance of the sample. All the spectra show the same type of semiconducting-like dependence rendering a maximum conductivity of 0.3 S/cm at 523 K. Thus, the atmosphere ($O_2$, Ar) does not seem to affect the electrical conductivity, as observed for $SrCoO_{3-y}$.[31]

An Arrhenius plot of the values obtained under oxygen (Figure 12a) and argon (Figure 12b) shows an almost identical trend. The linear dependence observed in the temperature range studied, i.e., 388−523 K, could indicate a thermally activated hopping polaron mechanism, as observed for the $Ba_{1-x}Sr_xCo_{1-y}Fe_yO_{3-\delta}$ system[32] with an activation energy of ∼0.3 eV under $O_2$ or Ar atmospheres. To confirm this behavior, we carried out an additional measurement under dry 5%$H_2$−Ar.

The impedance measurements under hydrogen, Figure 13, show at least one arc with a capacitance of $5 \times 10^{-10}$ F, which can be ascribed to the grain boundary of the material. The lower conductivity under reducing conditions evidence that $SrBaCo_2O_5$ exhibits a predominant p-type electronic conductivity. The conductivity in $O_2$ was 3 orders of magnitude higher compared to dry 5% $H_2$−Ar. It should be noted that the stability of the sample under 5% $H_2$ at 523 K is rather poor, with an increase of 100−200 Ω every hour.

The conductivity seems to be heavily affected by the substitution in the A- or B-site of $SrCoO_{3-y}$ to produce a cubic phase. The introduction of small amounts (5−10%) of elements such as $Sc^{3+}$ or $Sb^{5+}$ in the B-site of $SrCoO_{3-y}$ allows the stabilization of the cubic phase with high electrical conductivities under air, i.e,. 177 S/cm at 573 K for the Sc-doped[31] and 300 S/cm for the Sb-doped phase[33] at 673 K. From these temperatures, both doped materials exhibit metallic like behavior, which is fairly typical of cobaltites. The improvement in the conductivity may be due to a number of factors, though in the present case it seems that the stabilization of a highly conductive cubic phase[32] is responsible for such an increase; for the Sb-doped system, the introduction of $Sb^{5+}$ affects the Co oxidation state, leading to an increase in the electrical conductivity.

In our case, the introduction of 50% Ba in the A-site allows the same stabilization of the cubic phase but produces a decrease of about one order in the conductivity values, as observed in other cobaltites with identical substitutions in the A-site.[34] A negligible effect would be expected in the Co oxidation state because of the divalent nature of both ions, Sr and Ba, and thus the introduction of Ba (with a higher radius than Sr) probably produces a low-conductive cubic phase and together with the low relative density of the measured sample may explain the low values of conductivities obtained. To improve the electrical properties of these materials, we are now exploring different cationic Sr/Ba ratios in order to get the stabilization of the cubic $SrCoO_{2.5}$-type phase with the smallest amount of $Ba^{2+}$ doping in the A-site.

**Acknowledgment.** Financial support through research project MAT2007-61954 (Spain) is acknowledged. We are grateful to Dr. M.T Fernández-Díaz, Dr. V. Cabañas, Dr. M. Hernández, Dr. E. Matesanz and Dr. F. Conde for helpful assistance.

CM802606S

(29) Martine-López, M. J.; Alonso, J. A.; Cascais, M. T. *Z. Naturforsch, B* **2003**, *58*, 571.
(30) Roth, W. L. *Phys. Rev.* **1958**, *110*, 1333.
(31) Zheng, P.; Ran, R.; Chen, Z.; Zhou, W.; Gu, H.; Shao, Z.; Liu, S. *J. Alloys Compd.* **2007**, *455*, 465.
(32) Minh, N. *J. Am. Ceram. Soc.* **1993**, *76*, 563.
(33) Aguadero, A.; de la Calle, C.; Alonso, J. A.; Escudero, M. J.; Fernández-Díaz, M. T.; Daza, L. *Chem. Mater.* **2007**, *19*, 6437.
(34) Wei, B. *J. Eur. Ceram. Soc.* **2006**, *26*, 2827–2832.